

## 40. STRUCTURAL EVIDENCE FOR THE NATURE OF HIATAL GAPS IN THE UPPER CRETACEOUS TO HOLOCENE SUCCESSION RECOVERED FROM THE ERATOSTHENES SEAMOUNT<sup>1</sup>

Rachel Flecker,<sup>2</sup> Achim Kopf,<sup>3</sup> and Maria José Jurado-Rodríguez<sup>4,5</sup>

### ABSTRACT

Three sites (Sites 965, 966, 967) drilled into the Eratosthenes Seamount during Ocean Drilling Program Leg 160 recovered a Cretaceous to Pleistocene succession in which several stratigraphic gaps were identified. Some of these are associated with changes in depositional environment, whereas others have apparently identical lithofacies on either side of the hiatus. Four independent structural data sets were generated to ascertain the tectonic characteristics of each hiatal gap. These are bedding and fracture measurements on downhole formation microscanner data; bedding and fracture measurements on recovered core; strain data collected from individual marker particles in thin section; and axial ratio measurements of cross sections through burrows exposed on the split-core face. These data, in combination with lithostratigraphic and biostratigraphic information, indicate that, whereas most of the hiatuses were generated by tectonic events, some were generated by a combination of slow sedimentation, reworking, and possibly sediment bypassing. Furthermore, each drill site appears to be located on a different structural block that was affected by differential movement at least as far back as middle Eocene time.

### INTRODUCTION

The Eratosthenes Seamount is a prominent bathymetric feature (Limonov et al., 1994) located south of Cyprus in the Eastern Mediterranean (Fig. 1). It has been interpreted as a rifted fragment of Gondwana (Kempfer, 1993) that now, driven by incipient collision with Eurasia (Robertson, 1990; Woodside, 1991; Kempfer, 1993), is in the process of breaking up along a subduction zone south of Cyprus (Woodside, 1977; Le Pichon and Angelier, 1979; Rotstein and Kafka, 1982). One of the major objectives of Ocean Drilling Program (ODP) Leg 160 was to test this hypothesis by drilling a transect of holes across the structure (Fig. 1), permitting its tectonic history to be reconstructed.

The three sites located on the Eratosthenes Seamount were drilled into the plateau (Site 966), slope (Site 965), and foot (Site 967) of the edifice (Fig. 1). The sediments recovered ranged in age from Pleistocene to Cretaceous (Emeis, Robertson, Richter, et al., 1996), and a summary of the lithological (Emeis, Robertson, Richter, et al., 1996) and biostratigraphic (Emeis, Robertson, Richter, et al., 1996; Spezzaferri et al., Chap. 2, this volume; Premoli-Silva et al., Chap. 30, this volume) results is presented in Figure 2.

None of the successions drilled provide a full, unbroken, sedimentary record, first, because of poor recovery during drilling, and second, because each succession is interrupted by one or more stratigraphic hiatuses. The most profound of these hiatuses are between the upper Aptian and Cenomanian in Hole 967E (a gap of ~15 m.y.; Fig. 2), the Maastrichtian and Oligocene in Hole 967E (comprising ~34.5 m.y.), and beneath the Miocene extending to the Oligocene in Hole 967E and middle Eocene in Hole 966F (where in both cases at least 17 m.y. of stratigraphy is missing; Fig. 2). Other hiatuses with

shorter durations are located at the Miocene/Pliocene boundary in Holes 965A, 966F, and 967E, and within the Cenomanian to lower Turonian sediments in Hole 967E (Fig. 2).

Some of these stratigraphic gaps occur between contrasting lithologies (e.g., upper Aptian shallow-water carbonates overlain by Cenomanian abyssal sediments; Oligocene deep-water sediments overlain by neritic carbonates of Miocene age, which are in turn overlain by Pliocene deep-water marls and turbidites; Fig. 2; Emeis, Robertson, Richter, et al., 1996). These hiatuses were tentatively related to tectonic events (e.g., post-rift subsidence after the late Aptian; pre-collision shortening, uplift, and erosion caused by the onset of northward subduction in the Miocene; and subsidence caused by initial collision at the Miocene/Pliocene boundary; Robertson et al., 1996a). In other cases where little or no lithological change is visible across a stratigraphic gap (e.g., similar abyssal sediments occur on either side of the Maastrichtian-Oligocene hiatus in Hole 967E; Fig. 2), a period of nondeposition (Robertson et al., 1996a), or slow sedimentation combined with sediment reworking, has been envisaged (Premoli-Silva et al., Chap. 30, this volume).

All these interpretations are based exclusively on faunal and lithological information. The purpose of this paper is to compile, examine, and integrate the structural data obtained from the rocks bounded by these hiatuses as a means of elucidating the cause of each stratigraphic gap and hence the tectonic evolution of Eratosthenes. In particular, we wished to test the hypothesis that the three distinct blocks on which the different sites are located are bordered by faults that were reactivated throughout the history of the seamount. To this end, four independent structural data sets were generated. These are (1) bedding and fracture measurements on downhole formation microscanner (FMS) data; (2) bedding and fracture measurements on recovered core; (3) strain estimated from individual marker particle distributions in thin section; and (4) axial ratio measurements of cross sections through burrows exposed on the split-core face.

### METHODS

#### Formation MicroScanner

Formation MicroScanner (FMS) images are computer created, based on a dense matrix of electrical resistivity measurements of the borehole wall. During Leg 160, the slimhole FMS tool was used at

<sup>1</sup>Robertson, A.H.F., Emeis, K.-C., Richter, C., and Camerlenghi, A. (Eds.), 1998. *Proc. ODP, Sci. Results*, 160: College Station, TX (Ocean Drilling Program).

<sup>2</sup>Cambridge Arctic Shelf Programme, Department of Earth Sciences, University of Cambridge, Downing Street, Cambridge CB2 9EU, United Kingdom. rf211@esc.cam.ac.uk

<sup>3</sup>Geologisches Institut, Albert-Ludwigs Universität, Albertstrasse 23B, 79104 Freiburg, Federal Republic of Germany.

<sup>4</sup>Geophysikalisches Institut, Universität Karlsruhe, Hertzstrasse 16, D-76187 Karlsruhe, Federal Republic of Germany.

<sup>5</sup>Present address: Instituto de Ciencias de la Tierra (Jaume Almera) CSIC, Luis Sole Sabaris s/n, 08028, Barcelona, Spain.

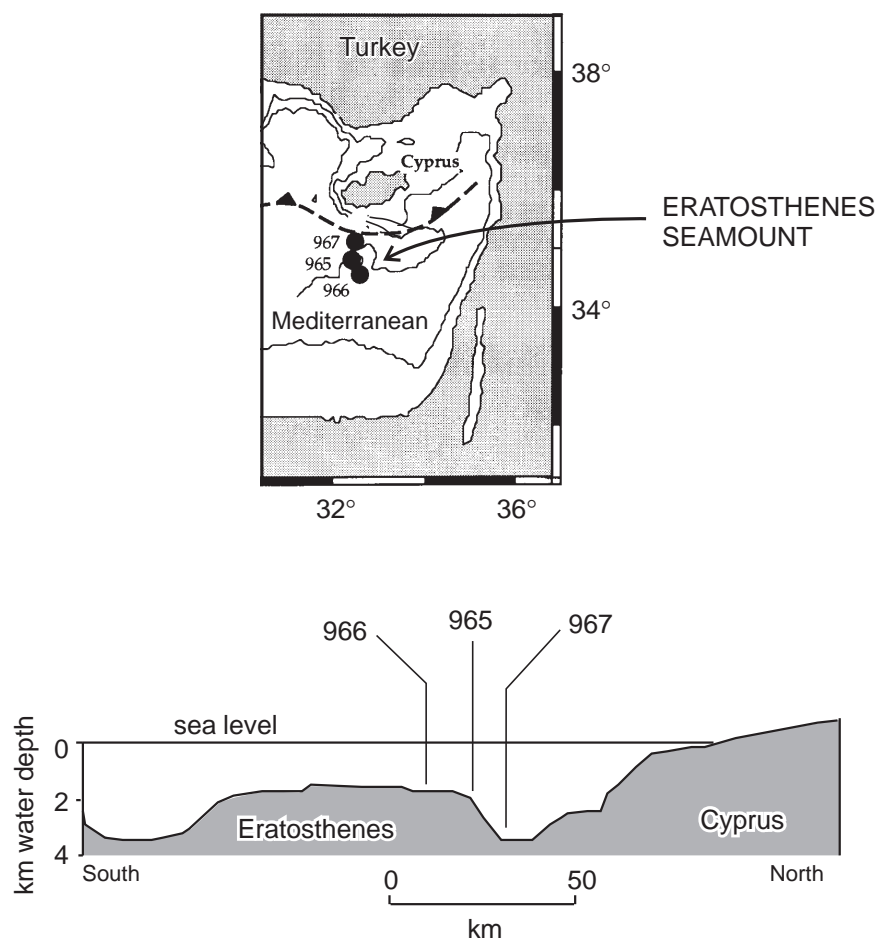


Figure 1. Map showing the location of the Eratosthenes Seamount and Sites 965, 966, and 967. The cross section illustrates the present-day bathymetric disposition of the seamount.

each of the Eratosthenes sites (Holes 965A, 966F, and 967E), providing a complete record of the borehole wall from between 60 and 70 m below seafloor (mbsf) to the base of each hole. The FMS tool measures microresistivity on four pads, generally providing up to 20% coverage of the borehole wall depending on hole geometry (Emeis, Robertson, Richter, et al., 1996). Electrical image processing was carried out on the data set (Harker et al., 1990; Ekstrom et al., 1987), and both static and dynamic normalization were applied to enhance images (Emeis, Robertson, Richter, et al., 1996; Jurado and Brudy, Chap. 41, this volume; Major et al., Chap. 38, this volume).

Interpretation of FMS images allowed the measurement of planar features crosscutting the borehole. Horizontal features appear flat on FMS images, whereas dipping planes plot as sine curves, the amplitude of which gives the dip angle. The azimuth of the plane is calculated at the low point of the sine curve and related to geographical coordinates using a fluxgate magnetometer. A detailed description of FMS methodology can be found in Jurado and Brudy (Chap. 41, this volume) and Major et al. (Chap. 38, this volume). These structural data were subdivided into bedding data (Table 1) and fracture data (Table 2).

A structural data set generated from FMS data has an inherent advantage over direct measurement of structural features on core, which is that FMS coverage is independent of the amount of core recovered (see below). However, not all structural features are equally visible in FMS data. Low-dipping surfaces and sealed fractures are

particularly difficult to identify. This leads to a measurement bias toward open fractures and steeply dipping surfaces.

### Strain Analysis Techniques on Thin Sections

Thin sections (oriented with the short axis of the section parallel to the core axis, and the long axis of the section randomly oriented with respect to geographic coordinates) were made of 59 carbonate samples of different age and depositional environment. Vertical shortening was estimated using three techniques: Fry; PODI; and Surfcor; the choice of technique was dependent on the availability of suitable marker particles. For both Fry and PODI, suitable detrital marker particles included organic matter, foraminiferal tests, and opaque minerals. The distribution of these particles in relation to each other is used to describe and quantify the sedimentary fabric in the two dimensions of the thin section.

The graphical method of Fry (1979; see Ramsay and Huber, 1983, for detailed description) is based on the length of vectors from the center of the marker particle to the centers of the 18 nearest-neighbor particles, assuming an initially statistically homogeneous particle distribution (e.g., Poisson distribution). A Fry diagram of the distribution of the neighboring particles with respect to the marker particle that is placed in the center as a reference point, is constructed. Assuming that the sample had an initial Poisson distribution, a marker-free area around the central particle is predicted for a strained sample.

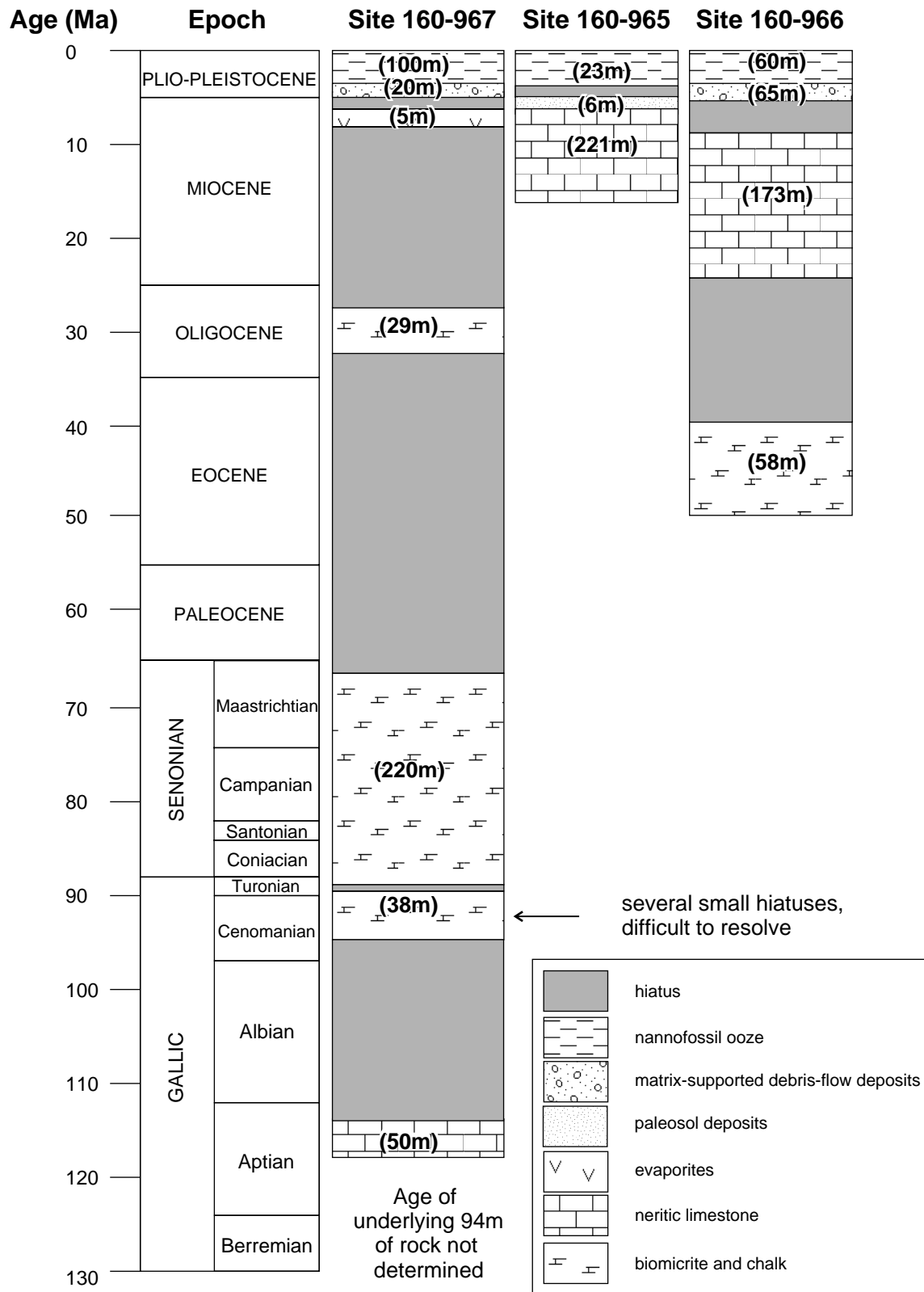


Figure 2. Simplified lithostratigraphic columns for Sites 965, 966, and 967 highlighting the number and duration of the hiatuses separating the recovered core. Numbers in brackets are the approximate thickness of sediment recovered for each interval. Biostratigraphic information is derived from Emeis, Robertson, Richter, et al. (1996), Premoli-Silva et al. (Chap. 30, this volume), and Spezzaferri et al. (Chap. 2, this volume).

**Table 1. Oriented bedding data derived from FMS data sets for Holes 965A, 966F, and 967E.**

This is a sample of the table that appears on the volume CD-ROM.

| Hole     | Depth (mbsf) | Azimuth | Dip  |
|----------|--------------|---------|------|
| 160-965A | 80.34        | 54.9    | 7.2  |
| 160-965A | 80.42        | 7.8     | 6.6  |
| 160-965A | 81.08        | 325.4   | 7.3  |
| 160-965A | 81.17        | 298.6   | 6.7  |
| 160-965A | 82.98        | 16.5    | 13.5 |
| 160-965A | 83           | 7.9     | 14   |
| 160-965A | 83.07        | 17.7    | 15.5 |
| 160-965A | 83.09        | 12.7    | 12.9 |
| 160-965A | 83.18        | 18.3    | 18.5 |
| 160-965A | 83.21        | 28.8    | 14.8 |

**Table 2. Oriented fracture data derived from FMS data sets for Holes 965A, 966F, and 967E.**

This is a sample of the table that appears on the volume CD-ROM.

| Hole     | Depth (mbsf) | Azimuth | Dip  |
|----------|--------------|---------|------|
| 160-965A | 77.7831      | 264.5   | 64.4 |
| 160-965A | 78.3763      | 114.2   | 54   |
| 160-965A | 79.4047      | 120.2   | 79.8 |
| 160-965A | 87.8312      | 177.6   | 85.3 |
| 160-965A | 89.1894      | 221.5   | 77.7 |
| 160-965A | 89.8005      | 183.2   | 73.4 |
| 160-965A | 95.78        | 192.7   | 82.3 |
| 160-965A | 100.16       | 114.3   | 76.1 |
| 160-965A | 101.642      | 98.1    | 74.8 |
| 160-965A | 101.812      | 100.2   | 74.9 |

The shape of this marker-free area is the strain ellipse, and from it the axial ratio ( $R_f$ ) can be calculated.

The PODI technique is based on measuring the frequency of marker particles at  $10^\circ$  intervals over the entire sample (Unzog, 1990). Once again, the assumption is that the particles were initially homogeneously distributed. For a fabric dominated by uniaxial shortening, a sine function with maximum marker particle abundance perpendicular to the core axis is the predicted result of PODI analysis. In reality, this is rarely achieved, and a best-fit sine function is derived from the population of marker particle spacings. From the amplitude of this sine function, the strain ellipse and its axial ratio ( $R_f$ ) can be calculated.

The Surfcor technique was used for larger marker particles, such as foraminifer tests. This method involves defining the shape of a particle with polygonal tangents. The particle is then rotated, and the tangents are projected at  $10^\circ$  intervals onto a reference line (see Panozzo, 1984, for a detailed description). The total length recorded on the reference line (i.e., the sum of the projected tangents) for each interval is plotted vs. the number of degrees rotated and results in a sine curve. The ratio between the maximum and minimum total projected lengths for a particle rotated by  $360^\circ$  is the axial ratio ( $R_f$ ) of the finite strain ellipse.

For all techniques, vertical shortening ( $e_v$ ) can be calculated from the axial ratio  $R_f$  following:

$$e_v = (1 / R_f) - 1 \quad (1)$$

These estimates of strain are conservative because thin sections are not necessarily oriented in the direction of maximum stress. The errors on these data are less than 0.15.

### Strain Analysis Techniques on Burrows

In addition to the strain estimates of marker particles in thin section, axial ratios ( $R_f$ ) of cross sections through burrows exposed on

the core face were also measured. Burrows occur in the middle Eocene, Oligocene, Miocene, and Pliocene successions on Eratosthenes (Emeis, Robertson, Richter, et al., 1996), and often appear to have been flattened. Because the pre-Pliocene carbonates were drilled using rotary (RCB) and extended (XCB) coring techniques, the orientation of the cut surface of each core with respect to geographic coordinates was not known, and was therefore assumed to have been randomly oriented. Similarly, the orientation of the burrows with respect to the core face is assumed to be random. The orientation of the long and short axes of the strain ellipse for an individual burrow were estimated visually, and the length of the burrow along each axis measured using a ruler. The axial ratio ( $R_f$ ) was then calculated. The mean  $R_f$  for each core was used in Equation 1 to calculate vertical shortening ( $e_v$ ). The strain estimated from burrows, like that deduced from thin section, is conservative because there is no constraint on the orientation of maximum strain.

### Core-Based Structures

The structural data set from Sites 965, 966, and 967 is taken directly from Emeis, Robertson, Richter, et al. (1996). Deformation data include measurements of faults, fractures, and veins, reported as dip angle and dip direction in core reference frame coordinates (see Emeis, Robertson, Richter, et al., 1996). Bedding information was also obtained from core, and occasionally indicated that tilting had occurred. Such intervals were checked against equivalent depth FMS data that generally corroborated and provided an orientation of the tilting. Because of the inability to reorient RCB and XCB core to geographical coordinates without paleomagnetic information, these data were excluded from the initial shipboard interpretation of the evolution of the Eratosthenes Seamount (Robertson et al., 1996a). A post-cruise paleomagnetic study on pre-Pliocene material was considered unfeasible because of the scale required to cope with the fragmentary nature of the recovered core.

Although structural features of core recovered during Leg 160 are without geographic coordinates (Emeis, Robertson, Richter, et al., 1996), their occurrence and nature provide information complementary to the FMS structural data set. The frequency of deformational features in the cores can be used as a measure of the intensity of small-scale deformation by relating the abundance of features to the quantity of recovered rock (i.e., [faults + fractures]/centimeters). These values retain an inherent measurement bias that is based on variable core recovery because it is presumed that the most intensely fractured rock was not recovered (MacLeod et al., 1994). For this reason, the percentage of core recovery is plotted alongside the frequency histogram on a core-by-core basis.

### DEFINITION OF STRATIGRAPHIC UNITS

Poor recovery and the absence of age-diagnostic fossils make the precise location of some stratigraphic boundaries difficult. A comparison of the units defined by lithostratigraphy (Emeis, Robertson, Richter, et al., 1996), biostratigraphy (Emeis, Robertson, Richter, et al., 1996; Premoli-Silva et al., Chap. 30, this volume; Spezzaferri et al., Chap. 2, this volume), and logging data (e.g., FMS, geological high-sensitivity magnetic tool, geochemical logging tool, and standard Quad combination logging tools employed by ODP; Emeis, Robertson, Richter, et al., 1996) illustrates that in general, the depths of unit boundaries concur within a few meters. Small discrepancies can be accounted for by the prerequisite comparison of a 100% log record with partial core recovery. Because this paper is primarily concerned with biostratigraphic gaps in the recovered succession, the biostratigraphic units were used wherever possible. Where the absence of age-diagnostic fossils precluded biostratigraphic designation, FMS-defined boundaries have been used.

## RESULTS

## Formation Microscanner

Interpretation of FMS data from Holes 965A, 966F, and 967E resulted in the compilation of extensive bedding and fracture data sets. Table 1 lists the bedding data derived from a preliminary examination of the FMS data from Holes 965A, 966F, and 967E. More detailed interpretation of a screened bedding data set is given in Jurado and Brudy (Chap. 41, this volume). Rose diagrams of bedding dip direction indicate that the Miocene strata in Hole 965A dip toward the northwest (Fig. 3) in contrast to the Miocene bedding recorded at Site 966, which indicate a predominantly northeast direction of dip (Fig. 4). These distributions are not observed in the data generated by Major et al. (Chap. 38, this volume). Mid-Eocene sediments in Hole 966F dip toward the northwest (Fig. 4). The Oligocene sediments of Hole 967E have a broad, bimodal, north-south distribution (Fig. 5), whereas the abundant bedding measurements from the Upper Cretaceous (upper Turonian to Maastrichtian) show no clear single dip direction (Fig. 5). In contrast, the upper Aptian sediments in Hole 967E dip unequivocally toward the south-southeast (Fig. 5). The few bedding planes measured from the Cenomanian-Turonian succession suggest that these sediments are also predominantly south-southeast-dipping (Fig. 5). The basal sediments (FMS Unit 6) of Hole 967E show a broad north-northwest-south-southeast bimodal distribution (Fig. 5).

Lower hemisphere stereographic plots of poles to fractures from this preliminary FMS data set (Table 2) for each unit can be seen in Figures 3, 4, and 5. Where data are sufficient, they have been contoured to illustrate fracture distribution.

East-west-striking fractures in Miocene sediments were identified at both Sites 966 (Fig. 4) and 965 (Fig. 3). The more abundant fracture data available for Hole 965A (Fig. 3) indicates that another set of broadly north-south-striking fractures also exists. Minimal data are available both for the middle Eocene sediments of Hole 966F (Fig. 4) and the Oligocene sediments of Hole 967E (Fig. 5). However, the distribution of numerous fractures in upper Turonian to Maastrichtian sediments of Hole 967E (Fig. 5) suggest they were affected by two orientations of fractures: one striking northeast-southwest and dipping predominantly to the southeast, and another striking northwest-southeast and dipping predominately to the northeast. Very few fractures were identified in sediments older than the late Turonian (Fig. 5).

## Structural Data from Split Cores

The paucity of fractures identified in the FMS images of the Oligocene strata at Site 967 (Fig. 5) is mirrored by the low frequency of faults and fractures observed in the core, as well as by the relatively high (33.9%–57.4%) recovery. The graph of fault, fracture, and vein abundance measured in the recovered core suggests that fault and fracture deformation at Site 967 generally affected sediments older than Maastrichtian (Fig. 5). The apparent abundance of veins in the upper Aptian sediments may well be exaggerated by low recovery. More abundant microfaults, fractures, and veins were observed in the middle Eocene sediments of Hole 966F (Fig. 4), in contrast to the apparently fractureless overlying Miocene carbonates.

## Strain Estimations

The uniaxial shortening, calculated by using Fry/PODI and Surf for techniques for the Miocene sediments of Hole 965A, show a relatively constant range of values (–15% to –45%; Table 3) irrespective of depth (i.e., down to 225 mbsf, Fig. 3). In Hole 967E a similar constancy of vertical shortening can be seen in the Oligocene and Upper Maastrichtian sediments (e.g., between –20% and –40% over the interval from 150 to 200 mbsf; Fig. 5, Table 3). However, in the underlying sediments (Campanian and older), vertical shortening shows an overall increase with depth (below 225 mbsf; Fig. 5) across the various hiatuses in the lower part of the succession (Fig. 2). The exception to this trend is a single measurement at the base of Hole 967E, which has a much lower vertical shortening value (–23%; Fig. 5) and is regarded as an outlier.

The values of vertical shortening for middle Eocene sediments in Hole 966F (Fig. 4; Table 4) and Oligocene sediments in Hole 967E (Fig. 5; Table 5) that were derived from the measurement of burrows, are significantly higher than those derived from PODI and Surf for strain techniques (see discussion below). However, the axial ratio values for the Miocene of Hole 966F are comparable to the values obtained from PODI and Surf for data for sediments drilled at Holes 965A and 967E at similar depths (100–300 mbsf). Furthermore, a linear increase in the vertical shortening can be seen at both Sites 966 and 967 in the burrow data. In Hole 966F, the degree of flattening increases from Pliocene sediments through the Miocene to Eocene sediments across the hiatus at the base of the Miocene. The wide range of strain values for burrows in Pliocene sediments from Site 967 may indicate slumping.

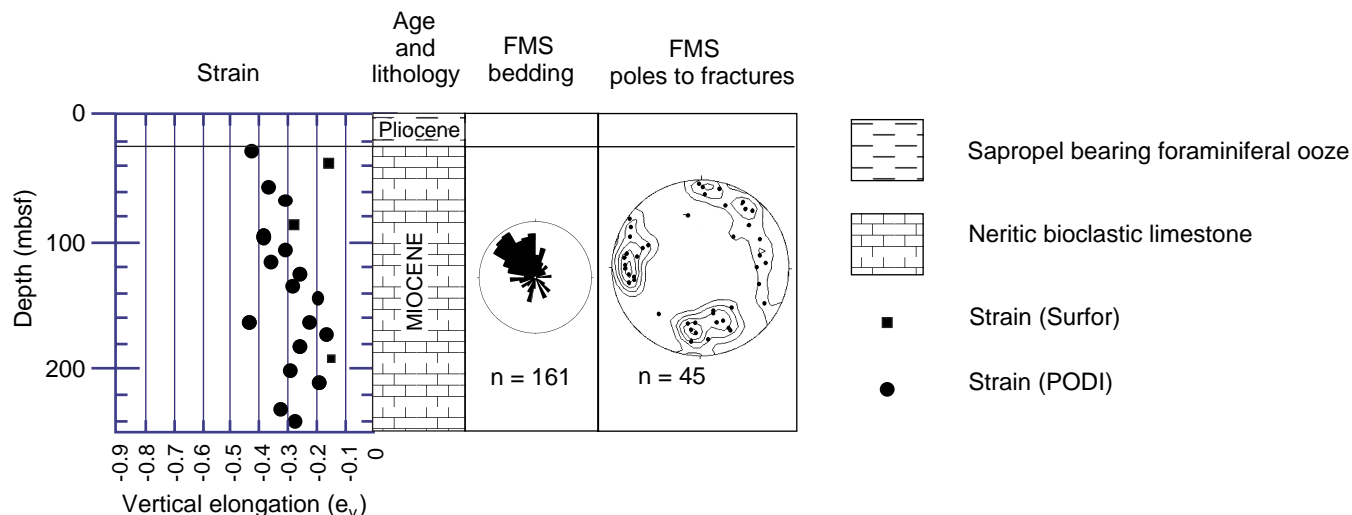


Figure 3. Lithological column for Hole 965A showing the strain (PODI and Surf for) data plotted vs. depth, a rose diagram of bedding dip direction derived from FMS data, and a contoured plot of poles to fractures also derived from FMS data.

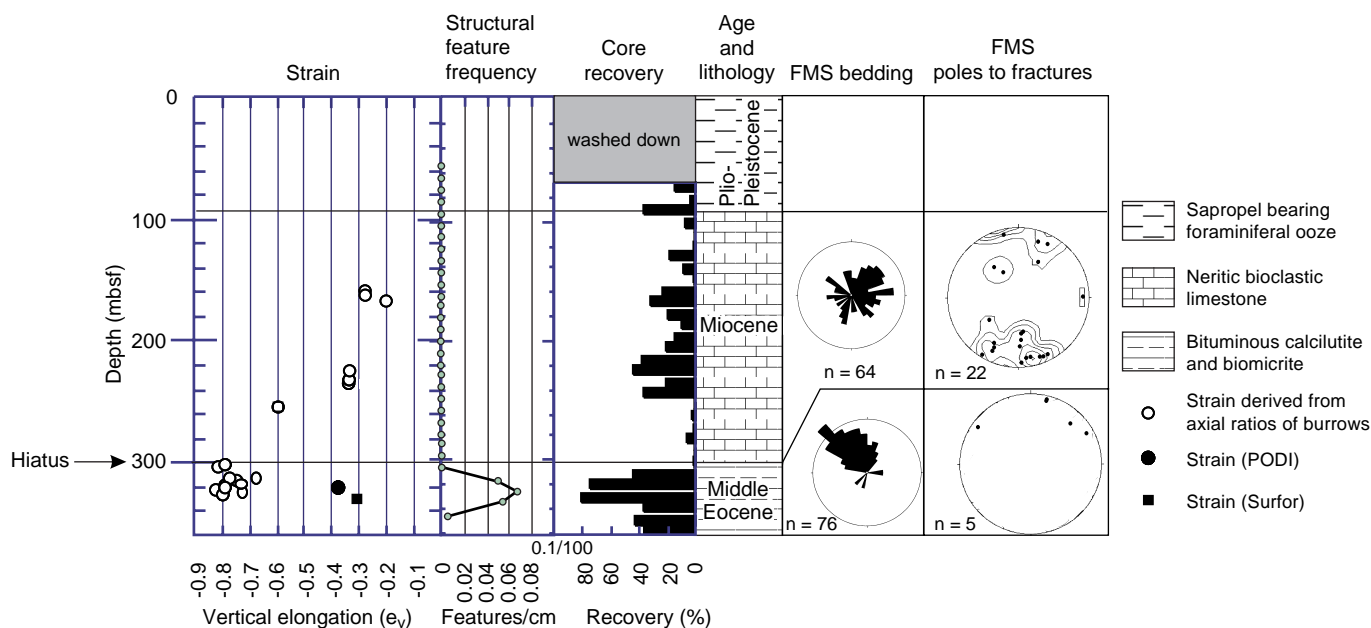


Figure 4. Lithological column for Site 966 showing the strain (PODI and Surfior) data plotted vs. depth, a plot of the frequency of structural features measured in core recovered from Hole 966F, a histogram of the percentage of core recovered from this hole, rose diagrams of bedding dip direction derived from FMS data in Hole 966F, and contoured plots of poles to fractures also derived from FMS data.

The results of the different strain estimates indicate that the overall vertical shortening behavior of the Miocene to Cretaceous carbonate sediments can be described by an approximately linear relationship with depth. The gradient of this line varies considerably (i.e., almost no shortening with depth at Site 965, Fig. 3, but approximately 8%–10% per 100 m for Hole 967E, Fig. 5, and ~32% per 100 m at Site 966, Fig. 4) and appears to depend on the technique used.

Shortly after the geometry of burrows was first used to study deformation (Crimes, 1975), the different response of carbonate sediments to stress was demonstrated (Byers and Stasko, 1978). Grain size and carbonate content have also been shown to have a profound effect on shortening behavior (e.g., Gaillard and Jautée, 1987; Audet, 1995). At Eratosthenes, both the carbonate and organic contents change significantly from burrow fill to surrounding material. Furthermore, the Miocene limestones have a coarser grain size than Eocene bituminous chinks. These differences help to explain the extreme flattening observed in the middle Eocene burrows at the base of Hole 966F (Fig. 4), and the difference between these estimates of vertical shortening and those derived from PODI and Surfior data for a similar interval (Fig. 4).

Given the overall linear increase in shortening, a linear porosity decrease with depth might have been expected. An approximately linear decrease in thermal neutron porosity was recorded in Hole 965A (Emeis, Robertson, Richter, et al., 1996), but at Holes 966F and 967E a more complicated pattern with marked changes in porosity at lithological boundaries can be seen. Broadly, this can be explained by the differing response of chalk and limestone to chemical changes associated with burial (Goldhammer, 1997).

## DISCUSSION

### Upper Aptian to Cenomanian Hiatus

This hiatus is only exposed in Hole 967E and is marked by a change in facies from shallow-water limestones to calcareous nannofossil oozes thought to have been deposited in abyssal-water depths (Emeis, Robertson, Richter, et al., 1996). A coherent south–southeast

orientation of bedding dips contrasts with the poorly defined bedding in the overlying Cretaceous units (Fig. 5). Podi and Surfior data increase slightly across the hiatus. The combination of the structural and lithological data suggests that this stratigraphic gap is likely to have been generated tectonically and to have occurred at the same time as the carbonate platform foundered (Fig. 6; Robertson et al., 1996b). A certain amount of reworking does seem to have characterized this boundary leading to the occurrence of upper Aptian neritic limestone clasts in deep-water oozes (I. Premoli-Silva, pers. comm., 1997).

### Intra-Turonian Hiatus

This hiatus (Fig. 2), only visible in Hole 967E, may span <1 m.y., and is not marked by any significant lithological change. Sparse FMS bedding data and negligible fracture data for the Cenomanian to lower Turonian sediments make any comparison of these structures on either side of the hiatus difficult and tentative. The abrupt increase in vein frequency below 400 mbsf (Fig. 5) is probably at least partially a result of low recovery. The Podi and Surfior data show little variation across this boundary. It is possible that recognition of this small hiatus results, in part, from low recovery. Reworking of the sediment may also have been a causative factor.

### Maastrichtian to Oligocene Hiatus

Hole 965A did not penetrate sediments sufficiently old to recover the Maastrichtian to Oligocene hiatus documented in Hole 967E (Fig. 2). The stratigraphy at Site 966 where no Oligocene sediments were recovered, but middle Eocene chinks were observed, suggests that if the hiatus itself is not entirely restricted to the area around Site 967, its duration varies over short distances.

The structural evidence supporting tectonic generation for this unconformity is limited. It consists of an increase in the frequency of faults, fractures, and veins in recovered core, and the contrast between the bimodal north–south dip orientations of Oligocene sediments and the more complex distribution in sediments of late Turo-

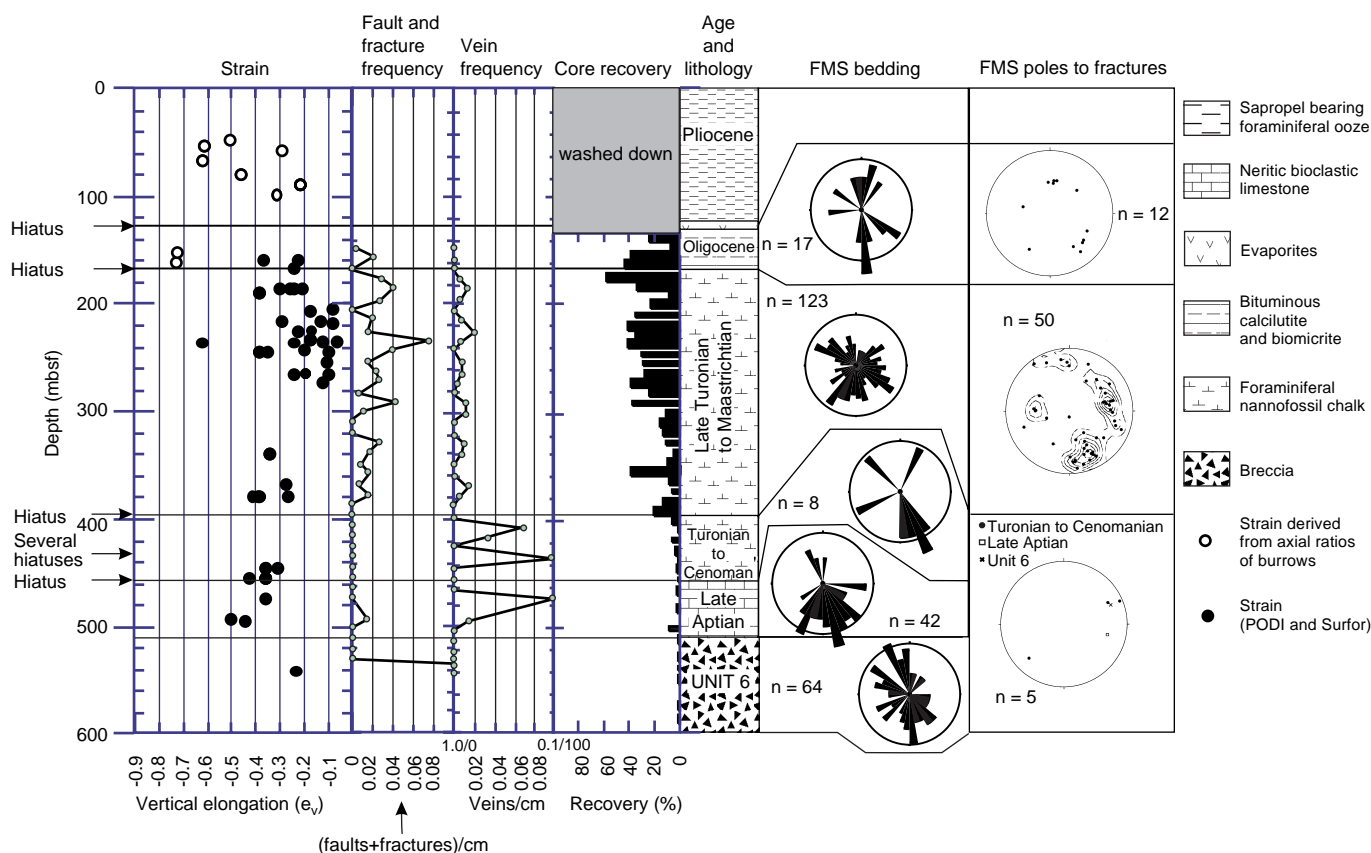


Figure 5. Lithological column for Site 967 showing the strain (PODI and Surfor) data plotted vs. depth, a plot of the frequency of faults and fractures measured in core recovered from Hole 967E and another of the frequency of veins, a histogram of the percentage of core recovered from this hole, rose diagrams of bedding dip direction derived from FMS data in Hole 967E, and contoured plots of poles to fractures also derived from FMS data.

Table 3. Strain data measured using PODI and Surfor techniques for Holes 965A, 966F, and 967E.

This is a sample of the table that appears on the volume CD-ROM.

| Core, section, interval (cm) | Depth (mbsf) | Number | $\theta$ (°) | Axial ratio, $R_f$ (PODI) | Vertical shortening, $e_v$ (PODI) | Axial ratio, $R_f$ (Surfor) | Vertical shortening, $e_v$ (Surfor) |
|------------------------------|--------------|--------|--------------|---------------------------|-----------------------------------|-----------------------------|-------------------------------------|
| 160-967E-                    |              |        |              |                           |                                   |                             |                                     |
| 6R-2, 62-70                  | 159.79       | 42     | 15.1         | 1.28                      | -0.21875                          | 1.28                        | -0.21875                            |
| 6R-3, 19-3                   | 160.62       | 219    | 18.2         | 1.58                      | -0.367088608                      |                             |                                     |
| 7R-1, 47-54                  | 167.77       | 117    | 15.5         | 1.31                      | -0.23664121                       |                             |                                     |
| 9R-1, 16-25                  | 186.66       | 54     | 8.2          | 1.42                      | -0.295774648                      | 1.42                        | -0.295774648                        |
| 9R-1, 38-44                  | 186.88       | 69     | 13.5         | 1.35                      | -0.259259259                      | 1.35                        | -0.259259259                        |
| 9R-1, 78-84                  | 187.28       | 68     | 19.9         | 1.26                      | -0.206349206                      | 1.26                        | -0.206349206                        |
| 9R-1, 100-104                | 187.50       | 69     | 20.7         | 1.31                      | -0.236641221                      | 1.31                        | -0.236641221                        |
| 9R-3, 96-100                 | 189.89       | 56     | 27.7         | 1.61                      | -0.378881988                      | 1.61                        | -0.378881988                        |
| 11R-1, 31-37                 | 206.11       | 44     | -12.5        | 1.09                      | -0.082568807                      | 1.09                        | -0.082568807                        |
| 11R-2, 33-38                 | 207.16       | 90     | 28.4         | 1.21                      | -0.173553719                      | 1.21                        | -0.173553719                        |

nian to Maastrichtian age (Fig. 5). Strain data suggest that contrasts within the Upper Cretaceous sediments are greater than those between sediments of Maastrichtian and Oligocene age. There is no apparent change in depositional environment across this protracted (~34.5 m.y.) hiatal gap. Figure 6 illustrates one possible explanation for such a large stratigraphic hiatus invoking slight topographic elevation of Site 967, combined with slow sedimentation, reworking, and possibly sediment bypassing.

### The Pre-Miocene Hiatus

The pre-Miocene hiatus extends to Oligocene sediments in Hole 967E and to middle Eocene sediments in Hole 966F (Fig. 2). Because

the only indication of Miocene sediments at Site 967 was the identification of a narrow interval of evaporites beneath Pliocene sediments by well logs (Emeis, Robertson, Richter, et al., 1996), no structural data are available for comparison with the underlying Oligocene succession. However, lithological contrasts at both Site 966 and 967 suggest that the pre-Miocene hiatus is marked by a transition from relatively deep-water facies (chalks of middle Eocene age in Hole 966F and Oligocene age in Hole 967E; Emeis, Robertson, Richter, et al., 1996) to a shallow marine or restricted hypersaline environment (Miocene neritic limestone in Hole 966F, evaporites in Hole 967E; Fig. 6).

At Site 966, several structural parameters differ across the Miocene/middle Eocene boundary. Bedding dip is toward the northeast in

**Table 4. Axial ratio measurements on burrows from Hole 966F and the resulting strain calculations.**

This is a sample of the table that appears on the volume CD-ROM.

| Hole     | Core | Section | Top of core (mbsf) | Bottom of core (mbsf) | Mean depth of core (mbsf) | y (parallel to the core axis; mm) | x (perpendicular to the core axis; mm) | Axial ratio ( $R_f = x/y$ ) | Mean $R_f$ | Vertical shortening ( $\epsilon_v$ ) |
|----------|------|---------|--------------------|-----------------------|---------------------------|-----------------------------------|--|-----------------------------|------------|--------------------------------------|
| 160-966F | 11R  |         |                    |                       |                           | 4                                 | 6                                      | 1.5                         |            |                                      |
| 160-966F | 11R  |         |                    |                       |                           | 8                                 | 10                                     | 1.25                        |            |                                      |
| 160-966F | 11R  |         | 153.8              | 173.1                 | 163.45                    |                                   |  | 2.75                        | 1.38       | -0.27                                |
| 160-966F | 12R  |         |                    |                       |                           | 4                                 | 5                                      | 1.25                        |            |                                      |
| 160-966F | 12R  |         |                    |                       |                           | 8                                 | 10                                     | 1.25                        |            |                                      |
| 160-966F | 12R  |         | 163.5              | 173.1                 | 168.3                     |                                   |  | 2.5                         | 1.25       | -0.2                                 |
| 160-966F | 18R  |         |                    |                       |                           | 8                                 | 16                                     | 2                           |            |                                      |
| 160-966F | 18R  |         |                    |                       |                           | 7                                 | 15                                     | 2.14                        |            |                                      |
| 160-966F | 18R  |         |                    |                       |                           | 10                                | 17                                     | 1.7                         |            |                                      |
| 160-966F | 18R  |         |                    |                       |                           | 8                                 | 6                                      | 0.75                        |            |                                      |

Note: See "Methods" section (this chapter) for more information.

**Table 5. Axial ratio measurements on burrows from Holes 967A, 967B, and 967E and the resulting strain calculations.**

This is a sample of the table that appears on the volume CD-ROM.

| Hole     | Core | Top of core (mbsf) | Bottom of core (mbsf) | Mean depth of core (mbsf) | y (parallel to the core axis; mm) | x (perpendicular to the core axis; mm) | Axial ratio ( $R_f = x/y$ ) | Mean $R_f$ | Vertical shortening ( $\epsilon_v$ ) |
|----------|------|--------------------|-----------------------|---------------------------|-----------------------------------|--|-----------------------------|------------|--------------------------------------|
| 160-967A | 6H   |                    |                       |                           | 6                                 | 18                                     | 3                           |            |                                      |
| 160-967A | 6H   |                    |                       |                           | 9                                 | 14                                     | 1.56                        |            |                                      |
| 160-967A | 6H   |                    |                       |                           | 5                                 | 17                                     | 3.4                         |            |                                      |
| 160-967A | 6H   |                    |                       |                           | 6                                 | 16                                     | 2.67                        |            |                                      |
| 160-967A | 6H   |                    |                       |                           | 12                                | 22                                     | 1.83                        |            |                                      |
| 160-967A | 6H   |                    |                       |                           | 7                                 | 20                                     | 2.86                        |            |                                      |
| 160-967A | 6H   | 53.3               | 54.8                  | 54.05                     |                                   |  |                             | 2.55       | -0.61                                |
| 160-967A | 9H   |                    |                       |                           | 11                                | 25                                     | 2.27                        |            |                                      |
| 160-967A | 9H   |                    |                       |                           | 8                                 | 20                                     | 2.5                         |            |                                      |
| 160-967A | 9H   |                    |                       |                           | 5                                 | 8                                      | 1.6                         |            |                                      |

Note: See the "Methods" section (this chapter) for more information.

Miocene sediments, and toward the northwest in middle Eocene sediments. The amount of shortening indicated by the axial ratios of burrows is significantly higher in middle Eocene sediments than in the overlying Miocene succession. The frequency of fractures, veins, and faults in recovered core is also higher in middle Eocene sediments.

The combination of the structural data and the large change in paleowater depth required by lithological contrasts therefore indicates that the pre-Miocene hiatus was tectonically induced. It seems probable that Oligocene sediments were deposited at Site 966 and subsequently removed (Fig. 6).

### Miocene to Pliocene Hiatus

This hiatus is observed in Holes 966F and 965A (Fig. 2). It occasions more notice than other packets of missing strata in the Eratosthenes record because of the link to the Messinian draw-down and evaporite deposition (Hsü et al., 1977). Evidence for the nature of this boundary has been documented elsewhere (Robertson et al., 1996a; Spezzaferri et al., Chap. 2, this volume) and a tectonically driven hiatus caused by subsidence and collapse as the seamount arrived at the Cyprus active margin seems unequivocal.

### Evidence of Persistent Block Faulting

The evidence for persistent independent behavior of the blocks making up the Eratosthenes Seamount comes in various forms. Where it is possible to compare units of similar age (i.e., the Miocene neritic carbonates recovered at Sites 966 and 965), the FMS bedding data indicate that the sediments dip consistently in different directions at each site (e.g., toward the northeast and northwest respectively; Figs. 3, 4). This may be the product of post-Miocene break up of the seamount as envisaged from the seismic lines generated to locate

Hole 965A ("Site 965" chapter, Emeis, Robertson, Richter, et al., 1996, fig. 8).

The differing stratigraphies at all three sites are another line of evidence, which support the concept of persistent block faulting. The absence of Miocene neritic carbonates at Site 967, although nearly 200 m was recovered at Sites 966 and 965 (Fig. 2) requires some explanation. A period of nondeposition through the Miocene is difficult to accept given the present relative bathymetries of the three sites (Fig. 1). The alternatives: (1) deposition followed by subsequent erosion, or (2) sediment bypassing, both necessitate differential movement between Site 967, and the two other Eratosthenes sites, either during, or before, the deposition of Pliocene sediments. Similarly, the distribution of Oligocene and middle Eocene sediments in Holes 967E and 966F (Fig. 2) is difficult to explain unless at times these sites were differentially prone to erosion and accumulation. It seems fairly clear, therefore, that differential motion on individual blocks drilled at Sites 967 and 966 occurred as far back as the middle Miocene. A schematic illustration of this is shown in Figure 6.

One possible explanation for the numerous relatively small hiatuses in the Cenomanian to Turonian sediments is that small-scale differential block movement generated relief for minor downslope reworking and possibly permitted localized sediment bypassing or contouring. Without recovery of sediments of comparable age elsewhere, it is not possible to test this hypothesis.

### CONCLUSIONS

Examination of lithological and structural data reveals that most of the hiatus gaps identified in the successions recovered from three sites on the Eratosthenes Seamount are likely to have been generated tectonically (i.e., Miocene-Pliocene hiatus, pre-Miocene hiatus, upper Aptian to Cenomanian hiatus). The prolonged hiatus between the

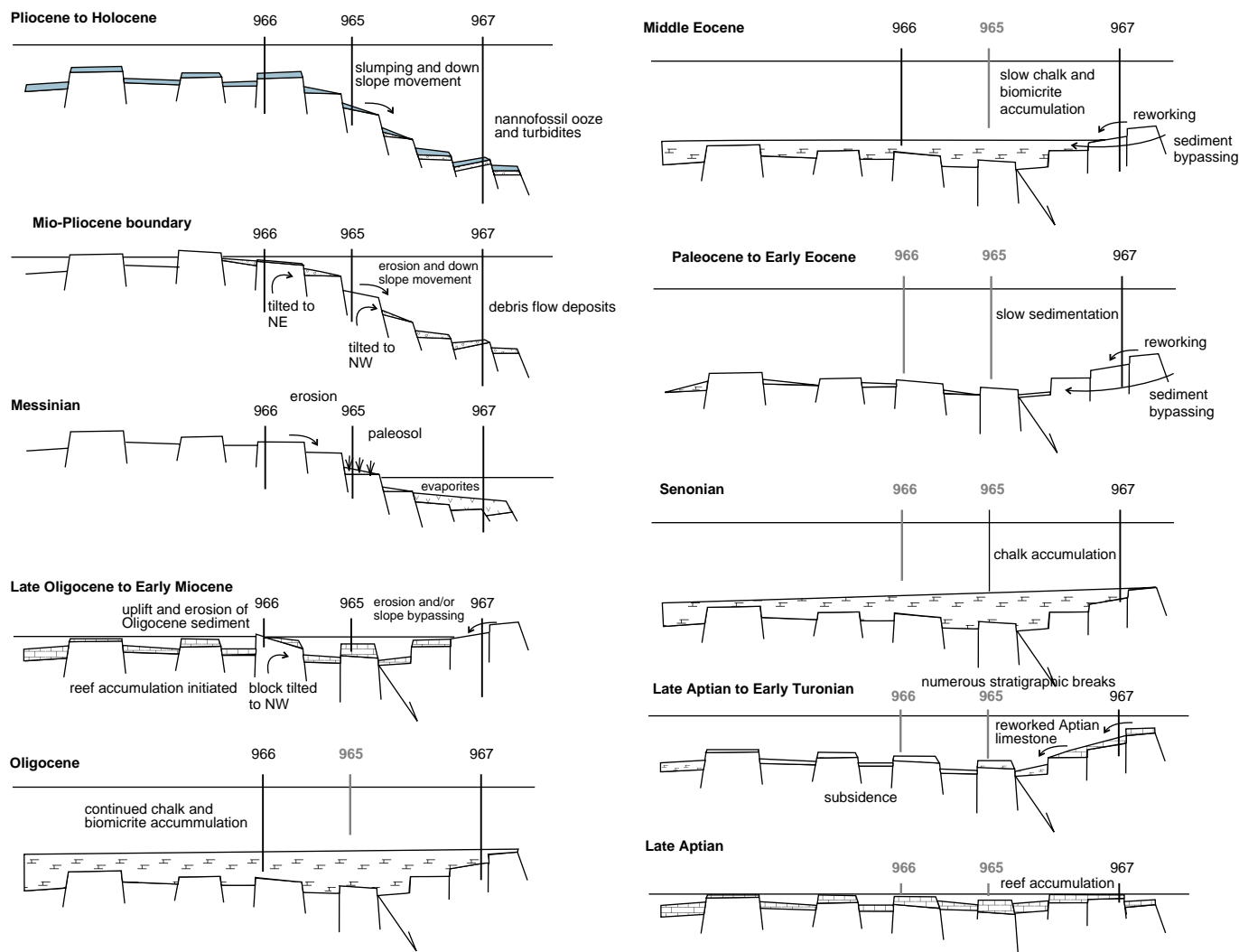


Figure 6. Schematic diagram illustrating the possible evolution of the Eratosthenes Seamount from Cretaceous to Holocene times. The model is based on the structural and stratigraphic information documented in the text for Sites 965, 966, and 967, and attempts to account for the recognized hiatuses. Most of the hiatuses are accompanied by significant change in facies indicating a tectonic element to the evolution (e.g., Oligocene to late Oligocene to early Miocene sketches). However the Oligocene, middle Eocene, and Paleocene to early Eocene sketches illustrate a scenario where a hiatus develops as a result of slow sedimentation, reworking, and sediment bypassing. The model also illustrates persistent independent movement of the blocks on which the three sites are located to account for differences in the recovered succession. Faded site numbers and drill locations indicate that drilling did not penetrate sediments of this age.

Maastrichtian and Oligocene sediments in Hole 967E is an exception. This hiatus may have been formed as a result of slow sedimentation, reworking, and possibly a component of sediment bypassing as a result of slight structural elevation. Several small hiatuses in Cenomanian and Turonian sediments are probably the result of reworking, if in fact they are not merely hiatuses simulated by low recovery.

The differing stratigraphic successions recovered from Eratosthenes, in combination with structural information and seismic data, suggest that each of the three sites is located on a different structural block. These blocks have acted independently of one another and undergone differential movement at least as far back as the middle Eocene.

#### ACKNOWLEDGMENTS

The authors would like to thank Isabella Premoli-Silva and Silvia Spezzaferri for keeping them up to date with the most recent biostratigraphy for Eratosthenes. The manuscript also benefited consid-

erably from the helpful reviews of Simon Allerton, Peter Clift and Alastair Robertson. Funding was provided for R. Flecker by Natural Environmental Research Council, for A. Kopf by Deutschen Forschungsgemeinschaft, research grant Be1041/10, and for M.J. Jurado-Rodríguez by European Union research grant ERB4001GT933623.

#### REFERENCES

- Audet, D.M., 1995. Modelling of porosity evolution and mechanical compaction of calcareous sediments. *Sedimentology*, 42:355–373.
- Byers, C.W., and Stasko, L.E., 1978. Trace fossils and sedimentologic interpretation—McGregor Member of the Platteville Formation (Ordovician) of Wisconsin. *J. Sediment. Petrol.*, 48:1303–1310.
- Crimes, T.P., 1975. The stratigraphical significance of trace fossils. In Frey, R.W. (Ed.), *The Study of Trace Fossils*: Berlin (Springer), 109–130.
- Ekstrom, M.P., Dahan, C., Chen, M.-Y., Lloyd, P., and Rossi, D.J., 1987. Formation imaging with microelectrical scanning arrays. *Log Analyst*, 28:294–306.
- Emeis, K.-C., Robertson, A.H.F., Richter, C., et al., 1996. *Proc. ODP, Init. Repts.*, 160: College Station, TX (Ocean Drilling Program).

- Fry, N., 1979. Random point distribution and strain measurements in rocks. *Tectonophysics*, 60:89–106.
- Gaillard, C., and Jautée, E., 1987. The use of burrows to detect compaction and sliding in fine-grained sediments: an example from the Cretaceous of SE France. *Sedimentology*, 34:585–593.
- Goldhammer, R.K., 1997. Compaction and decompaction algorithms for sedimentary carbonates. *J. Sediment. Res.*, 67:26–35.
- Harker, S.D., McGann, G.J., Bourke, L.T., and Adams, J.T., 1990. Methodology of Formation Micro Scanner image interpretation in Claymore and Scapa Fields (North Sea). In Hurst, A., Lovell, M.A., and Morton, A.C. (Eds.), *Geological Applications of Wireline Logs*. Geol. Soc. Spec. Publ. London, 48:11–25.
- Hsü, K., Montadert, L., Bernoulli, D., Cita, M.B., Erickson, A., Garrison, R.E., Kidd, R.B., Melieres, F., Müller, C., Wright, R.C., 1977. History of the Mediterranean salinity crisis. *Nature*, 267:399–403.
- Kempler, D., 1993. Tectonic patterns in the Eastern Mediterranean [Ph.D. thesis]. Hebrew Univ., Jerusalem.
- Le Pichon, X., and Angelier, J., 1979. The Hellenic arc and trench system: a key to the neotectonic evolution of the eastern Mediterranean area. *Tectonophysics*, 60:1–42.
- Limonov, A.F., Woodside, J.M., and Ivanov, M.K. (Eds.), 1994. *Mud Volcanism in the Mediterranean and Black Seas and Shallow Structure of the Eratosthenes Seamount: Initial Results of the Geological and Geophysical Investigations during the Third "Training-through-Research" Cruise of the R/V Gelendzhik (June–July 1993)*. UNESCO Rep. Mar. Sci., 64.
- MacLeod, C., Parson, L.M., and Sager, W.W., 1994. Reorientation of cores using the Formation MicroScanner and Borehole Televiewer: application to structural and paleomagnetic studies with the Ocean Drilling Program. In Hawkins, J., Parson, L., Allan, J., et al., *Proc. ODP, Sci. Results*, 135: College Station, TX (Ocean Drilling Program), 301–309.
- Panozzo, R., 1984. Two-dimensional strain from the orientation of lines in a plane. *J. Struct. Geol.*, 6:215–221.
- Ramsay, J.G., and Huber, M.I., 1983. *The Techniques of Modern Structural Geology* (Vol. 1): *Strain Analysis*: London (Acad. Press).
- Robertson, A.H.F., 1990. Tectonic evolution of Cyprus. In Malpas, J., Moores, E.M., Panayiotou, A., and Xenophontos, C. (Eds.), *Ophiolites: Oceanic Crustal Analogues*. Proc. Symp. "Troodos 1987": Nicosia, Cyprus (Geol. Surv. Dep., Minist. Agric. Nat. Resour.), 235–250.
- Robertson, A.H.F., and Shipboard Scientific Party, 1996a. Role of the Eratosthenes Seamount in collisional processes in the Eastern Mediterranean. In Emeis, K.-C., Robertson, A.H.F., Richter, C., et al., *Proc. ODP, Init. Repts.*, 160: College Station, TX (Ocean Drilling Program), 513–520.
- , 1996b. Tectonic introduction. In Emeis, K.-C., Robertson, A.H.F., Richter, C., et al., *Proc. ODP, Init. Repts.*, 160: College Station, TX (Ocean Drilling Program), 5–20.
- Rotstein, Y., and Kafka, A.L., 1982. Seismotectonics of the Cyprean Arc, Eastern Mediterranean Region: subduction, collision and arc jumping. *J. Geophys. Res.*, 87:7694–7707.
- Unzog, W., 1990. Beispiele von Strainanalysen in Kristallingebieten. In *TSK III, 3. Symposium für Tektonik, Strukturgeologie und Kristallingeologie*. Kurzfassungen der Vorträge und Poster, Graz, 265–266.
- Woodside, J.M., 1977. Tectonic elements and crust of the eastern Mediterranean Sea. *Mar. Geophys. Res.*, 3:317–354.
- , 1991. Disruption of the African Plate margin in the eastern Mediterranean. In Salem, M.J., Sbeta, A.M., Bakbak, M., and Rida, M. (Eds.), *The Geology of Libya*: Symp. Geol. Libya 3, 6:2319–2329.

**Date of initial receipt: 10 January 1997**

**Date of acceptance: 26 August 1997**

**Ms 160SR-029**